Adsorption energy engineering of nickel oxide hybrid nanosheets for high areal capacity flexible lithium-ion batteries

Author

Huang, Yongchao, Yang, Hao, Xiong, Tuzhi, Adekoya, David, Qiu, Weitao, Wang, Zhongmin, Zhang, Shanqing, Balogun (Jie Tang), M-Sadeeq

Published

2020

Journal Title

Energy Storage Materials

Version

Accepted Manuscript (AM)

DOI

10.1016/j.ensm.2019.11.001

Adsorption Energy Engineering of Nickel Oxide Hybrid Nanosheets for High Areal Capacity Flexible Lithium-Ion Batteries

Yongchao Huang [b,1], Hao Yang [c,1], Tuzhi Xiong [a,1], David Adekoya[d], Weitao Qiu [c], Zhongmin Wang[e,*], Shanqing Zhang[d,*], M.-Sadeeq Balogun (Jie Tang) [a,*]

[a]College of Materials Science and Engineering, Hunan University, Changsha 410082, China.

[b]Institute of Environmental Research at Greater Bay, Key Laboratory for Water Quality and Conservation of the Pearl River Delta, Ministry of Education, Guangzhou University, Guangzhou 510006, People's Republic of China

[c]MOE of the Key Laboratory of Bioinorganic and Synthetic Chemistry, The Key Lab of Low-carbon Chemistry & Energy Conservation of Guangdong Province, KLGHEI of Environment and Energy Chemistry, School of Materials Science and Engineering, School of Chemistry, Sun Yat-sen University, Guangzhou 510275, China.

[d]Centre for Clean Environment and Energy, Griffith School of Environment, Gold Coast Campus, Griffith University, QLD 4222, Australia.

[e]School of Materials Science and Engineering, Guilin University of Electronic Technology, Guilin, 541004, P.R. China.

Corresponding Authors E-mail: zmwang@guet.edu.cn; s.zhang@griffith.edu.au; balogun@hnu.edu.cn

Abstract

Enriching electrode materials with definite functions is of great influence but highly challenging towards achieving high areal capacity lithium ion batteries (LIBs). Taking transition metal oxides (TMOs) as a case study, several attempts have been employed to demonstrate the large variations in lithium storage performance of TMOs, but explanation of the adsorption capability is rarely reported. Herein, the Li-ion storage chemistry of NiO nanosheets is successfully enhanced by modulating the position of the p-orbital energy level via engineering with porous N-doped carbon fiber and carbon quantum dots (CDs). The as-prepared *monolithic* NiO hybrid nanosheets (denoted CF/ECF/NiO/CD) exhibit high reversible areal capacity of 3.97 mAh cm^{-2} at 0.25 mA cm^{-2}, excellent cyclic stability with capacity of 2.91 mAh cm^{-2} at 3.0 mA cm^{-2}, as well as attractive rate capacity of 2.61 mAh cm^{-2} at 6.0 mA cm^{-2}. *In situ* Raman analyses, XPS, and DFT calculations reveal that performance enhancement is related to the electronic modulations between NiO, porous carbon fiber and CDs that triggers the shift of the p-band towards accommodating interfacial electron transfer that helps in promoting the Li storage activity. In addition, an all-flexible lithium ion battery based on CF/ECF/NiO/CD anode is assembled and a volumetric energy density of 619.9 Wh L^{-1} is achieved (equivalent to an energy density of 201.7 Wh kg^{-1}). This work opens an achievable approach for high-areal-capacity LIBs and provides relevant understanding into designing other LIB electrodes and beyond.

Keywords

monolithic electrode, high areal capacity, electronic interaction, adsorption energy, density functional theory

1. Introduction

Considering the future application of lithium ion batteries (LIBs) in the area of consumer electronics, aerospace, vehicle electrification, LIBs with high areal capacities require serious alleviation, but the main challenge is the electrode materials [1-4]. Due to the high theoretical capacities of transition metal oxides (TMOs) as anode materials for LIBs [5-7], extensive recognition has been given to them but their dependability towards practical application relics a critical challenge [8-10]. Especially in most cases that these TMO electrodes are usually prepared in their powdery forms and their Li storage performance is evaluated based on the active materials [11, 12], this could create undesirable inactive volume and uneven electrochemical environment for Li storage reactions. Additionally, it usually leads to the use of low mass loading of the active materials, tediousness in battery electrode fabrication and as a result, more-time consumption for electrode preparation and low areal capacity will be achieved [11, 13]. In such condition, it remains a crucial challenge to essentially design TMO electrode with distinct features that could display high areal capacity coupled with stable cycle life [14, 15].

To embrace this challenge, most reports adopted the design of TMOs nanostructures on three dimensional (3D) current collectors such as transition metal foams, conductive carbon based substrates [11, 12, 16-20] etc. The major contest is the issue of poor adhesion of active materials on these 3D substrates due to weak interaction leading to peeling-off of active material from the substrates after continuous lithiation processes [21, 22]. Taking NiO as a case study, Li et al. recently constructed 3D layer-by-layer NiO-based freestanding structures obtained from partial oxidation of NF, which could reinforces adhesion with active layer, contributes to the capacity of the whole electrode and delivers an areal capacity of 1.98 mAh cm^{-2} at 1.20 mA cm^{-2} [11]. With the impressive advancement accomplished with 3D NiO, their overall Li storage performance still requires further improvement [11, 12, 15, 17]. In addition, a large variation in performance of TMOs has been reported, but the underlying mechanism towards understanding these variations, especially in terms of the fundamental modulation and adsorption ability of the TMOs metal centers for Li storage attracts less understanding.

Herein, we favourably modulate NiO nanosheets as flexible anode for high areal capacity LIB by engineering the p-orbital through the design of *monolithic* or *all-in-one* multishell architecture. The *all-in-one* architecture consists of flexible carbon fiber coated with exfoliated porous N-doped carbon fiber (denoted CF/ECF) current collector (as capacity contributor), NiO nanosheets (as active layer) and carbon quantum dots (CDs) (as stabilizer) (denoted CF/ECF/NiO/CD). The multishell CF/ECF/NiO/CD shows excellent Li storage performance as anode material for LIB half-cell delivering an initial and reversible areal capacity up to 4.33 and 3.97 mAh cm^{-2} at 0.25 mA cm^{-2}, respectively, areal capacity of 2.91 mAh cm^{-2} at 3.0 mA cm^{-2} as well as attractive rate capability capacity of 2.61 mAh cm^{-2} at 6.0 mA cm^{-2}. In-situ Raman spectra, XPS analyses and density functional theory (DFT) calculations persistently show that the enhanced capacity, excellent conductivity and outstanding stability of CF/ECF/NiO/CD electrode cannot be attributed only to the synergistic effect, monolithic nature and capacity contribution from the CF/ECF current collector, but also the shift of p-orbital center, which enables the modulation of Li-ion diffusion pathway and interfacial electron transfer. This work provides helpful insights for enhancing the areal capacity of LIB and interpreting the large variation in the performance of TMOs via orbital engineering.

2. Experimental

2.1. Materials

Carbon textile was purchased from Fuel Cell Earth LLC, United States. $Ni(NO_3)_2$ $6H_2O$, Hexamethylene, concentrated HNO_3, NH_4VO_3, sucrose and ethanol (99.7%) were all purchased from Guangzhou Chemical Reagent Factory and used as received without further purification.

2.2. Synthesis of the CF/ECF

CF/ECF was prepared according to our previous report. [22] In a typical synthesis, after the cleaning of commercial carbon fiber (CF) in concentrated HNO_3, distilled water and ethanol for several times, the clean CF was immersed in a 30 min well–stirred solution of 10 mmol $Ni(NO_3)_2$ $6H_2O$ and 20 mmol Hexamethylene (HMT) dissolved in 40 mL of deionized water and vigorously stirred for another 10 min. The solution and CF were transferred to a 50 mL Teflon-lined stainless-steel autoclave and heated in an electric oven with a heating speed of 10 ^oC min^{-1} to 120 ℃ and maintained in an oven for 10 h and then allow naturally to cool to room temperature. After cooling down to room temperature, the Ni precursor/CF was washed with water, ethanol for several times and dried in 60 ^oC oven overnight and annealed in N_2 atmosphere at 900 ^oC for 90 min with heating speed of 10 ^oC min^{-1} to 900 ℃ (1 bar, 200 sccm). The product obtained after annealing was then immersed in conc. HCl for 12 hours to remove the Ni NPs and obtain porous exfoliated N-doped carbon cloth (denoted as CF/ECF).

2.3. Synthesis of CF/ECF/NiO

CF/ECF/NiO was formed by using as-prepared CF/ECF as a starting substrate and the hydrothermal growth for the Ni precursor was repeated. The product derived was then annealed in air at 500 ℃ for 3 h with heating rate of 10 ℃ min^{-1} to obtain the final product CF/ECF/NiO.

2.4. Synthesis of CF/ECF/NiO/CD

First carbon dots (CD) solution was prepared according to a previous work. [23] In a typical synthesis, 3.42g sucrose was dissolved in 100 mL of distilled water and the solution was transferred to a 100 mL Teflon-lined autoclave. The autoclave was heated in an electric oven at 160 ^{o}C for 3 h, and then allowed the electric oven to cool to room temperature. Upon cooling, the solution undergoes centrifugation and dried at 80 ^{o}C for 24 hours to obtain the CD powder. The CD powder obtained was dispersed in ethanol (99.99%) through ultra-sonication, and then centrifuged to collect the residue and precipitate solution. CF/ECF/NiO was immersed in the precipitated solution obtained for 6 h. After 6 h, the sample was removed from the precipitated solution and directly dried in the electric oven at 60 ^{o}C overnight to obtain CF/ECF/NiO/CD.

2.5. Synthesis of CF/NiO

CF@NiO was prepared exactly the same way as the CF/ECF/NiO but CF was used as the substrate instead of the CF/ECF.

2.6. Characterization

Field emission SEM (JSM-6330F) and transmission electron microscope (TEM) (JEM2010-HR, 200 KV) were used to characterize the morphology, structure, and composition of the samples. X-ray Photoelectron spectroscopy (XPS, ESCALab250) was used for element identification and heteroatom functional group distribution. X-ray diffraction Spectrometry (XRD; Shimadzu X-ray diffractometer 6000, Cu Kαradiation, Shimadzu, Tokyo, Japan) and Raman Spectroscopy (Renishaw inVia) were used to characterize the crystallographic information and phase purity of the samples.

2.7. Electrochemical Measurement

The lithium storage performance tests were carried out via CR2032 coin type cells. The electrodes were first cut into many smaller square pieces with the diameter of area of 1.0 cm^2. The working electrodes, CF/NiO, CF/ECF/NiO and CF/ECF/NiO/CD, lithium foil (serving as the counter and reference electrode) and Celgard 2400 separator to separate the electrodes. The mass loading of the CF/NiO, CF/ECF/NiO and CF/ECF/NiO/CD electrodes based on the entire area of 1.0 cm^2 are 12.20, 10.54 and 10.58 mg cm^{-2}, respectively. The batteries were assembled in an argon-filled glove box [Mikrouna (China) Co., Ltd.] with an organic liquid electrolyte that consists of 1 M $LiPF_6$ in 1:1 by volume of ethylene carbonate (EC)/dimethyl carbonate (DMC) was used. The cells were aged for 8-10 h before electrochemical test. The discharge and charge measurements were carried out on a Neware battery tester (CT-3008-164, Shenzhen, China). The voltage range for the battery testing are 0.01-3.0 V (vs. Li/Li^+) for the anode and 2.0-4.0 V (vs. Li/Li^+) for the cathode. The storage capacities were calculated based on current*hour per unit area i.e. mAh cm^{-2}. Cyclic voltammetry (CV) were conducted on electrochemical working station (CHI 1040c, Chenhua, Shanghai) at a scan rate of 0.1 mV s^{-1}. Electrochemical impedance spectroscopy (EIS) was measured on an AC voltage of 5 mV amplitude in the frequency range from 100 kHz to 0.1 Hz using an electrochemical workstation (CHI660D, Chenhua, Shanghai). The tests were carried out after the cells were assembled before and after cycling.

2.8. Assembling of the flexible lithium ion battery (FLIB) and storage measurement.

Commercial $LiNiCoMnO_2$ (LNCMO) purchased from Shenzhen Kejing Star Technology Co., LTD, was employed as the cathode. 4 cm × 6 cm Anodes (CF/NiO and CF/ECF/NiO/CD) and CF/ECF/LNCMO cathode with mass loading of 81 and 222 mg was synthesised, respectively. Based on our previous work, CF/ECF/LNCMO could deliver a capacity of 265 mAh g^{-1} [22]. The theoretical capacity of NiO is 720 mAh g^{-1}. The criterion for the mass ratio between is that we utilized about 3 folds of the LNCMO cathode material to match the capacity of the anode. Nickel strip was attached to both electrodes as current collectors. The electrolyte used is 1 M $LiPF_6$ in 1:1 by volume of ethylene carbonate (EC)/dimethyl carbonate (DMC), while the separator used to separate anode from cathode is also Celgard 2400 separator. All the battery components assembled into aluminium bag and sealed in the argon-filled glove box. The total weight of the FLIB device is 308 mg and the thickness is 0.1 cm. The potential range for testing the FLIB is 2.0 - 4.0 V. Cyclic voltammetry (CV) were conducted on electrochemical working station (CHI 1040c, Chenhua, Shanghai) at a scan rate of 0.1 mV s^{-1}. The storage capacities were calculated based on current*hour per unit area i.e. mAh g^{-1}, mAh cm^{-2} and mAh cm^{-3}. The lithium storage measurement of the battery was tested by applying direct current values of 5.0, 10.0 and 15.0 mA also using Neware battery tester (CT-3008-164, Shenzhen, China). The batteries were first cycled for 10 cycles to maintain its stability and avoid other side reactions. The electrochemical data reported for the FLIB are data recorded after initial 10 electrochemical cycles. The volumetric and mass energy densities were also calculated.

2.9. Computational Methodology

The entire calculations have been performed with the Vienna ab initio Simulation Package (VASP) [24]. 3D periodic boundary conditions were used to simulate the infinitely large systems. The vacuum space between sheets was adjusted to 20 Å to prevent the two membrane layers interaction. The fibre Brillouin zone was sampled by 1 × 3 × 1 k-points. The system electronic structure was manipulated using the generalized gradient approximation with the PBE functional [25]. The van der Waals interactions were added to the standard DFT description by Grimme's D2 scheme [26]. All calculations include spin polarization. During the entire calculations, the convergence parameters were 10^{-6} eV for the energy, 0.01 eV $Å^{-1}$ for the forces and an energy cut-off of 500 eV. A Gaussian smearing of 0.05 eV was also applied. Charge analysis was performed via Bader analysis [27], which included the core charges and charge density difference analysis within VASP.

3. Results

3.1. Morphological and Composition Characterization

CF/ECF/NiO/CD *monolithic* flexible anode was designed via hydrothermal, annealing and chemical bath reactions so as to address the issue of developing high areal capacity LIBs as shown in Figure 1a-i-ii. To achieve this, CF/ECF/NiO/CD was designed using porous and N-doped exfoliated flexible carbon fiber (CF/ECF) as substrate.

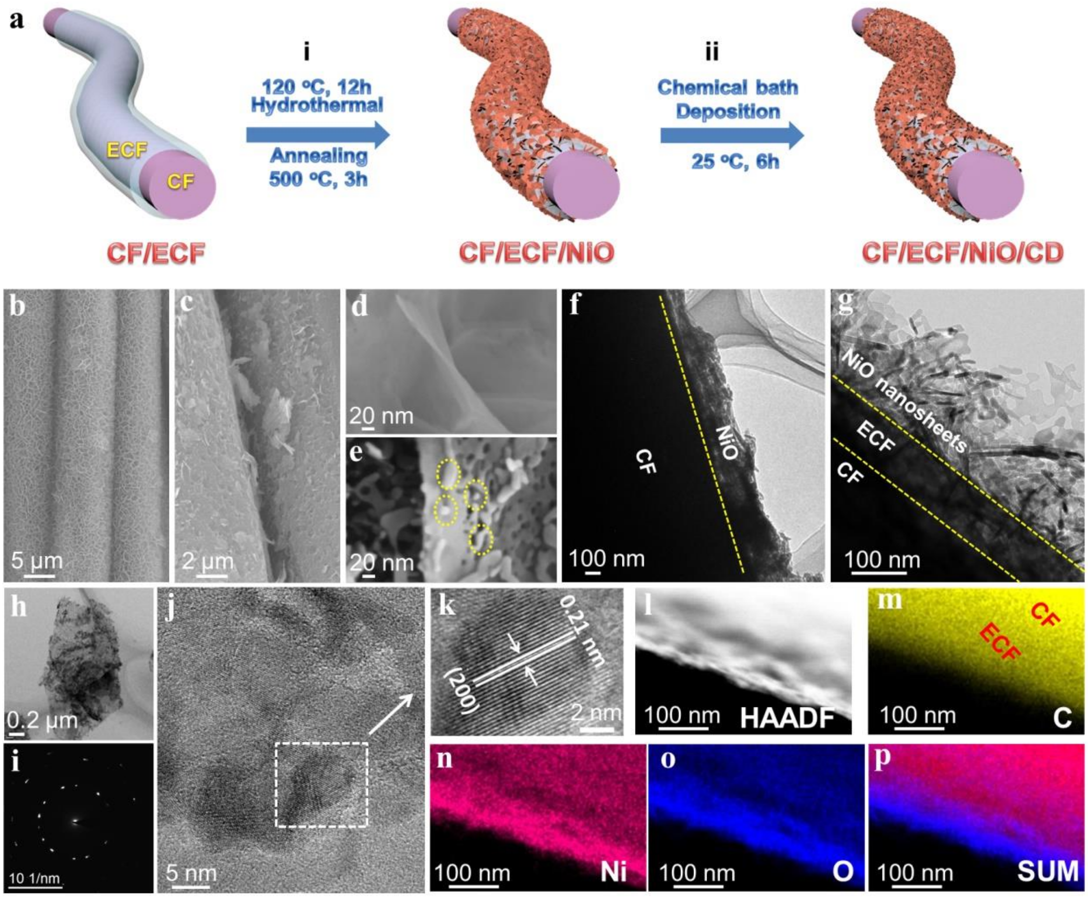

Fig. 1. Synthesis and Morphological characterization of the hybrids. a) Synthetic process of (i) NiO nanosheets on CF/ECF (CF/ECF/NiO) and (ii) CDs on CF/ECF/NiO (CF/ECF/NiO/CD). b) SEM image of CF/ECF/NiO/CD. c) SEM image of CF/ECF/NiO/CD showing the contact of CC@EC and NiO nanosheets. d) Magnified SEM image of CF/NiO and e) Magnified SEM image of CF/ECF/NiO/CD showing the CDs. TEM images of f) CF/NiO and g) CF/ECF/NiO/CD. h) Low magnification TEM image and i) corresponding SAED of CF/ECF/NiO/CD nanosheets. j) HRTEM image of NiO nanosheet from CF/ECF/NiO/CD showing 2d lattices. k) HRTEM image of CF/ECF/NiO/CD obtained from the dotted box in "h" showing lattice fringes of 0.21 nm corresponding to (200) phase of cubic NiO. l-p) Elemental mapping of CF/ECF/NiO/CD obtained from HRTEM image.

The porous and exfoliated surface of CF/ECF can be clearly seen and identified in the Supporting Information, Figure S1a-b. We hypothesize that CF/ECF should not only act as a current collector/substrate for the growth of

NiO nanosheets (Figure 1a) but also to contribute to the capacity of the battery [22, 28]. The weight of CF reduces after treatments (Figure S1d-g), indicating that the CF/ECF current collector is lighter in weight than bare CF, and does not lose its mechanical and flexible properties either (Figure S1c). According to scanning electron microscopy (SEM) analysis, uniform nanosheets of NiO were formed on the CF/ECF current collector (Figure 1b). The fabrication process of CF/NiO can be seen in Figure S2a. Similar nanosheets morphology was also formed on the CF current collector (Figure S2b). The NiO nanosheets adhered strictly to the surface of CF/ECF, indicating excellent binding interaction between the current collector and the NiO nanosheets (Figure 1c) [22], while the reverse remains the case for CF/NiO (details in Figure S3). For CF/ECF/NiO and CF/NiO samples, the surface of the nanosheets are very smooth (Figure 1d and S2b-c), respectively. After the insertion of CF/ECF/NiO sample to CDs solution via simple chemical bath process, CDs were deposited on the surface of the nanosheets (Figure 1e). The carbon dots were characterized using photoluminescence (PL) emission spectra as shown in Figure S4. The emission from the CDs continuously shifted to the higher wavelengths and the intensities of the shifted wavelength also varies. Such shift indicates emission of the surface-defects from the CDs. [29]

Transmission electron microscopy (TEM) studies were performed to investigate the core-triple layer architecture of CF/ECF/NiO/CD. According to Figure 1f, the nanosheets have no intimate interaction with the CF in the CF/NiO sample. However, the TEM image of CF/ECF/NiO/CD shows that the nanosheets are strictly bound and connected to the ECF (Figure 1g and enlarge image in Figure S5). The HRTEM images collected from CF/ECF/NiO/CD nanosheets (Figure 1h) shows the 2d lattices of NiO nanosheets (Figures 1j, S6a and S6c), while that of CF/NiO also displays similar trend (Figure S2d-e). Selected Area Electron Diffraction (SAED) collected from the entire NiO nanosheets confirms the polycrystalline nature of the nanosheet (Figures 1i, S6b and S6d), while SAED collected from each different NiO nanoparticles shows the single crystalline nature of the nanoparticles (Figure S6e) with lattice fringes of 0.21 nm corresponding to the (200) phase of NiO (JCPDS N: 47-1049) (Figures 1k and S6f). Moreover, atomic number of CD is much less than the average atomic number of NiO. According to the contrast mechanism in TEM, while the CD overlaps with NiO, it should not be observable. Moreover, results from the energy dispersive X-ray spectrometry (EDS) mapping analysis also affirmed the layer by layer architecture of CF/ECF/NiO/CD hybrid (Figure 1l-p). The entire SEM, TEM and EDS results justified the formation of the CF/ECF/NiO/CD nanosheets hybrid.

X-ray diffraction (XRD) pattern of CF/NiO, CF/ECF/NiO and CF/ECF/NiO/CD are shown in Figure S7 and confirmed the presence of both carbon and NiO phases in all the samples. Compared to the pristine CF/NiO, the three major XRD phases of NiO shifted to the higher degree theta in both CF/ECF/NiO and CF/ECF/NiO/CD, suggesting electronic interaction between the current collector and NiO. [22] Additionally, the results obtained from the Raman spectra revealed that the ratio of the defect carbon (D band) and graphitic carbon (G-band) i.e. D:G value of CF/ECF/NiO is significantly higher than that of CF/NiO due to the more defects and modification of the CF/ECF current collector (Figure S8) [22, 28]. Furthermore, X-ray photo spectroscopy (XPS) analyses of the three samples affirmed the presence of C, Ni and O (Figure S9a) but both CF/ECF/NiO and CF/ECF/NiO/CD are characterized with N 1s peak confirming the presence of N in the complex hybrids originating from the formation of CF/ECF substrate (Figure S9b). The results obtained from the O 1s XPS spectra of the three samples show that apart from the characteristics peaks of lattice oxygen (Ni-O) and defect oxygen (defect O), the O 1s XPS spectra of CF/ECF/NiO/CD possesses a new peak at 533.3 eV assigned to C-OH from the CDs [30, 31] and confirm the formation of CDs (Figure S9c). The entire XRD, Raman and XPS studies also affirmed the successful formation of CF/ECF/NiO/CD.

3.2. Lithium Storage Properties

The lithium storage properties of CF/NiO, CF/ECF/NiO and CF/ECF/NiO/CD were studied using them as working electrode and Li-foil as both counter and reference electrode. The 1st-3rd cyclic voltammetry (CV) curves of the electrodes at scan rate of 0.1 mV s^{-1} were compared in Figure S10. The CV curves of the electrodes were used to discuss the mechanism of lithium intercalation. Owing to the capacity contribution from CC substrate, the three electrodes (CF/NiO, CF/ECF/NiO and CF/ECF/NiO/CD) displayed both Li-ion conversion and insertion reactions from the NiO and CF or CC/ECF, respectively. Thus, the Li-ion conversion and insertion reactions of NiO and CF are displayed in eq. 1 and 2 [17, 32];

$$NiO + 2Li^+ + 2e^- \rightleftharpoons Ni + Li_2O \qquad (1)$$

$$C_6 + Li^+ + e^- \rightleftharpoons LiC_6 \qquad (2)$$

In eq. (1), according to the 1st electrochemical discharge cycle, elemental Ni and Li_2O were formed indicating the conversion reaction from NiO. [17, 32] In addition, both CF and CF/ECF exhibits full insertion mechanism [22, 28]. For the 1st-3rd curve, the CV curve surface area and peak current densities of CF/ECF/NiO/CD is the highest and strongest among the electrodes (Figure S11a-c) indicating higher electrochemical reactivity and capacity than both CF/NiO and CF/ECF/NiO.

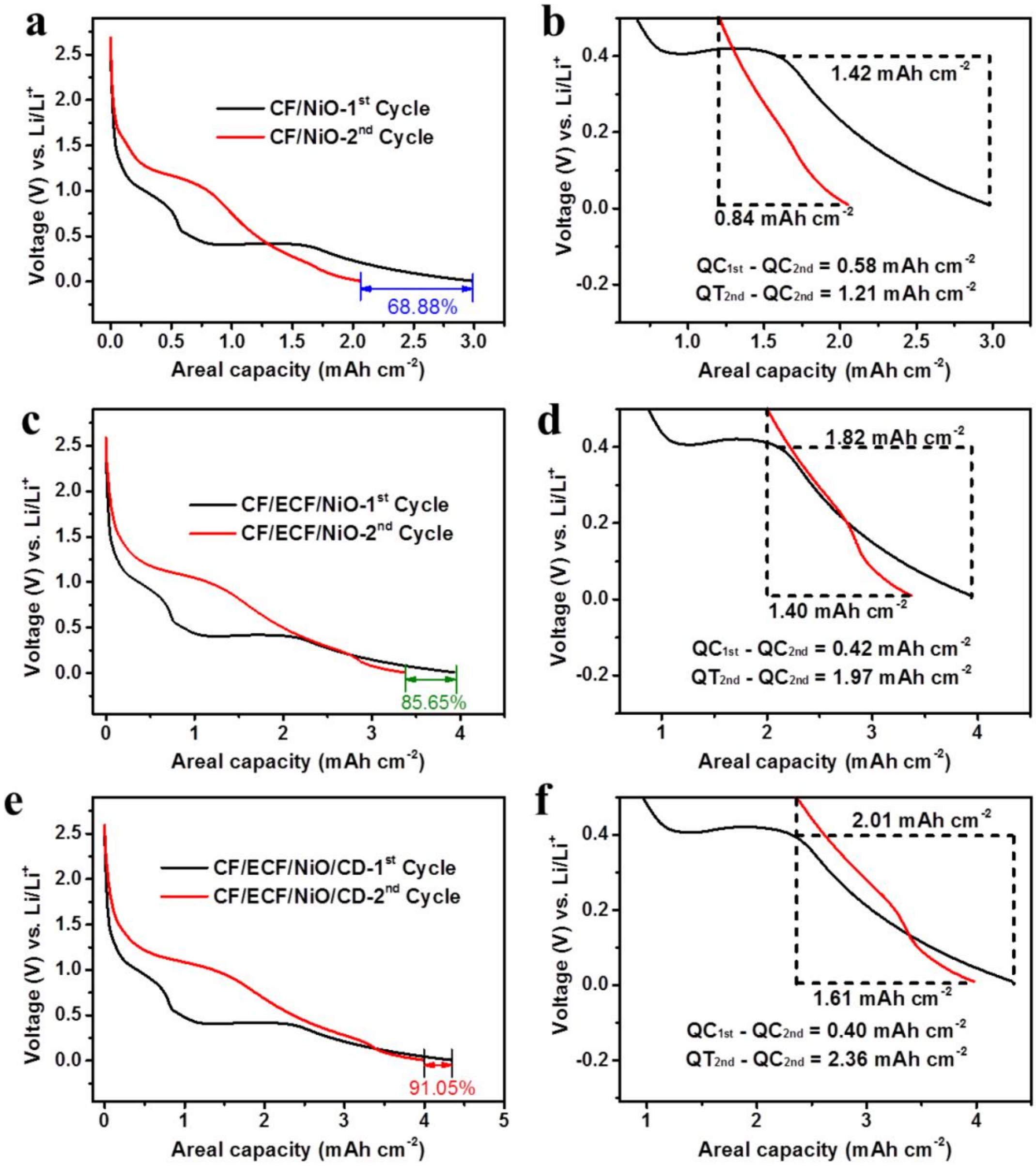

Fig. 2. Capacity contribution of CF/ECF and NiO. a) 1st and 2nd discharge profiles of CF/NiO. b) Discharge profiles between 0.5 V and 0.01 V showing the capacity contribution of CF/ECF/NiO electrode. c) 1st and 2nd discharge profiles of CF/ECF/NiO. d) Discharge profiles between 0.5 V and 0.01 V showing the capacity contribution of CF/NiO electrode. e) 1st and 2nd discharge profiles of CF/ECF/NiO/CD. f) Discharge profiles between 0.5 V and 0.01 V showing the capacity contribution of CF/ECF/NiO/CD.

Moreover, the 2nd and 3rd cycle CV curves of CF/ECF/NiO/CD electrodes are nearly the same suggesting high coulombic efficiency (CE). It should be pointed out that initial CE is one of the major problems of conversion reaction-based electrode materials owing to the formation of solid electrolyte interface (SEI) layer formation that causes large volume expansion and irreversible capacity loss [33-35]. Thus, the CE of CF/ECF/NiO/CD is about 87% during the first electrochemical cycle and increases to nearly 98% after subsequent cycling (Figure S11a), which is higher than those of CF/ECF/NiO (Figure S11b) and CF/NiO (Figure S11c) confirming the CV results in Figure S10. Hence, the multihybrid CF/ECF/NiO/CD system addresses the issue of poor initial CE.

Due to the higher electrochemical reactivity of CF/ECF/NiO/CD, the 1st and 2nd cycle discharge capacities of CF/ECF/NiO/CD are 4.33 and 3.97 mAh cm^{-2} which are slightly higher than those of CF/ECF/NiO (3.93 and 3.36 mAh cm^{-2}) and undoubtedly higher than that of CF/NiO (2.97 and 2.05 mAh cm^{-2}), respectively (Figures 2a,c,e and S11d-e). We believe that the higher capacity of CF/ECF/NiO/CD and CF/ECF/NiO can be associated with the capacity contribution from CF/ECF. To verify this, firstly, the Li-ion storage properties of CF and CF/ECF were also carried out to have detail information on the contribution of the carbon fiber. According to Figure S12, the storage performance of CF/ECF is better than that of pristine CF. The results suggest that CF/ECF did not only displays superior performance than CF but will also contribute to the performance of CF/ECF-based electrodes than pristine CF-based electrodes. Further analysis upon intercalation of Li-ion into the CF and CF/ECF below 0.5 V are studied using 1st and 2nd discharge processes because Li-ion are usually intercalated into CF matrix below 0.5 V [36-39]. The loss in the capacity contribution of carbon fiber current collectors (denoted as QC_{1st}-QC_{2nd}) in CF/NiO is

0.58 mAh cm^{-2} (Figure 2b), which reduces to 0.42 mAh cm^{-2} in CF/ECF/NiO (Figure 2d) and 0.40 mAh cm^{-2} in CF/ECF/NiO/CD (Figure 2f) indicating the CF/ECF is highly resistant to losing much capacity upon SEI layer formation [22, 28, 40]. The results also imply that the capacity contributed from NiO nanosheets (denoted as QT_{2nd}-QC_{2nd}) increases from 1.21 mAh cm^{-2} in CF/NiO to 1.97 mAh cm^{-2} in CF/ECF/NiO and 2.36 mAh cm^{-2} in CF/ECF/NiO/CD. Despite both CF/ECF/NiO and CF/ECF/NiO/CD electrodes benefit from the capacity contribution from CF/ECF current collectors, the areal capacity of CF/ECF/NiO/CD tends to be higher than CF/ECF/NiO, which can be attributed to the coating of CDs on the nanosheets surface. As it is well known that most TMOs exhibits poor conductivity and stability [6, 41], the coating of CDs could not only be used to enhance the conductivity of NiO nanosheets but also as a stabilizer for the entire multihybrid system. [23, 42] This further identifies that coating of CDs could enhance the CE and capacity of CF/ECF/NiO/CD and also helpful in enhancing its conductivity and stability. Hence, the capacity loss after the 2nd discharge cycle is 91% for CF/ECF/NiO/CD electrode (Figure 2e) and unquestionably superior to those of CF/NiO (69%, Figure 2a) and CF/ECF/NiO (86%, Figure 2c).

High-rate capability and excellent stability are crucial factors towards achieving high areal capacity LIBs. According to Figure 3a, CF/ECF/NiO/CD displayed continuous superiority in performance over CF/NiO and CF/ECF/NiO at different current densities ranging from 0.25 mA cm^{-2} to 6.0 mA cm^{-2}. Both CF/ECF/NiO and CF/ECF/NiO/CD display nearly the same capacity at current density of 0.25 mA cm^{-2}. However, CF/ECF/NiO/CD delivers a high areal capacity of 2.61 mAh cm^{-2} at current density of 6.0 mA cm^{-2}, which outshine that those of CF/ECF/NiO (1.25 mAh cm^{-2}), CF/NiO (0.24 mAh cm^{-2}) and recently reported areal capacity-based electrodes [11, 20, 43]. The excellent rate performance of CF/ECF/NiO/CD is associated with enhanced and rapid kinetics owing to the coating of the CDs that could act as useful stabilizer.

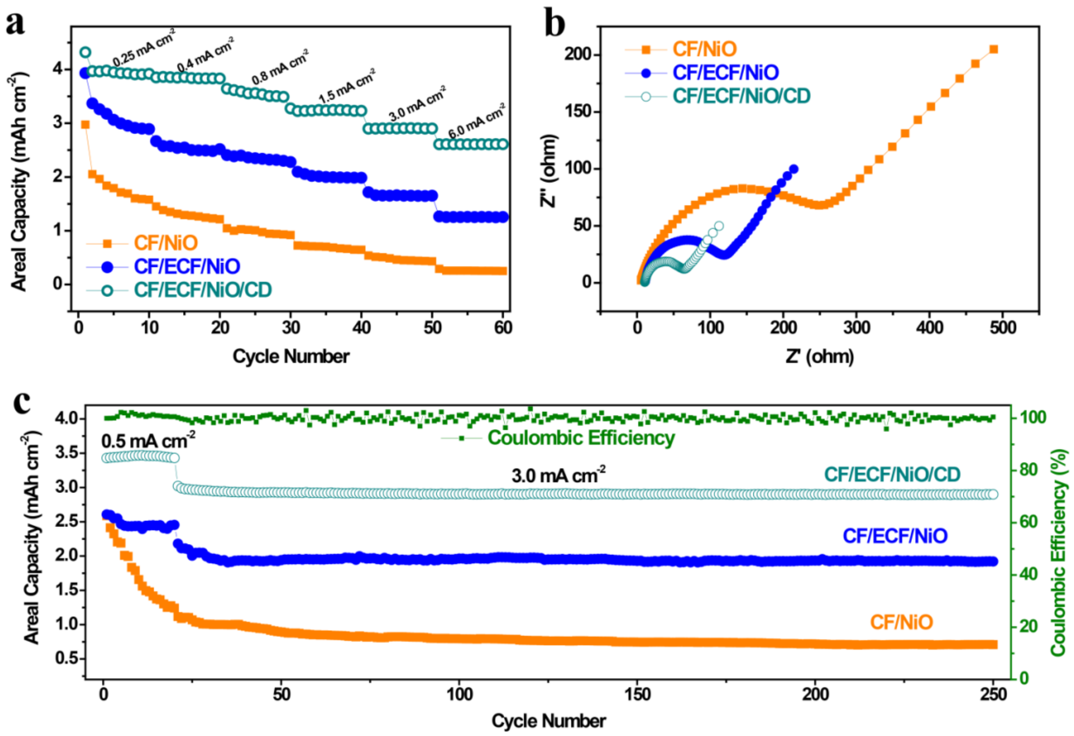

Fig. 3. Lithium storage Properties. a) Rate capability, b) Nyquist plot and c) cyclic stability of CF/NiO, CF/ECF/NiO and CF/ECF/NiO/CD electrodes.

The electrochemical impedance spectroscopy (EIS) analysis provide further information on the kinetics of the electrodes revealing that the semi-circle in the Nyquist plots of the electrodes represent the charge transfer resistance (R_{ct}, i.e. the smaller the semi-circle, the better the kinetics). Thus, CF/ECF/NiO/CD cell displayed the smallest R_{ct} (64.5 Ω) compared to CF/ECF/NiO (119.1 Ω) and CF/NiO (255.1 Ω) (Figure 3b) suggesting superior kinetics of CF/ECF/NiO/CD over its counterparts. The EIS results additionally affirm that CDs coating could be the reasons for high-rate performance in CF/ECF/NiO/CD electrode. Furthermore, CF/ECF/NiO/CD electrode continues to display outstanding stability up to 250 cycles at current density of 3.0

mA cm^{-2} retaining an areal capacity of 2.91 mAh cm^{-2} and outperformed those of CF/ECF/NiO (1.92 mAh cm^{-2}) and CF/NiO (0.71 mAh cm^{-2}) (Figure 3c). One important factor is that compared to CF/NiO (displaying continuous and drastic capacity deterioration between the 1st and 50th electrochemical cycling) and CF/ECF/NiO (showing slow capacity deterioration between the 1st and 50th electrochemical cycling), CF/ECF/NiO/CD could achieve no capacity deterioration upon the entire electrochemical stability cycles. By comparing the SEM morphological images of both CF/NiO and CF/ECF/NiO/CD after stability test, the nanosheets morphology of NiO can still be maintained justifying the excellent stability of CF/ECF/NiO/CD electrode (Figure S13a), while those of CF/NiO have been destroyed (Figure S13b). These results also confirms that the NiO nanosheets have intimate interaction with the CF/ECF but have little or no intimate interaction with the CF. Likewise, there exists less variation in the kinetics of CF/ECF/NiO/CD electrode as well (Figure S14). Hence, the excellent Li-storage performance of CF/ECF/NiO/CD electrode can not only be credited to the capacity contribution and excellent conductivity of the CF/ECF current collector but also the introduction of efficient CDs stabilizer.

3.3. In situ Raman Study

To have further insight on the capacity contribution from CF/ECF towards achieving high areal capacity LIBs, *in situ* Raman spectra analysis was performed for CF/NiO and CF/ECF/NiO/CD cells during the 2nd discharge cycle. The *in situ* Raman spectra analysis could be simultaneously used to study the degradation mechanism for the discharge capacity of CF/NiO. Firstly, according to Figures 2 and 3, electrochemical analyses have shown that the CF/ECF/NiO and CF/ECF/NiO/CD shows better performance than CF/NiO.

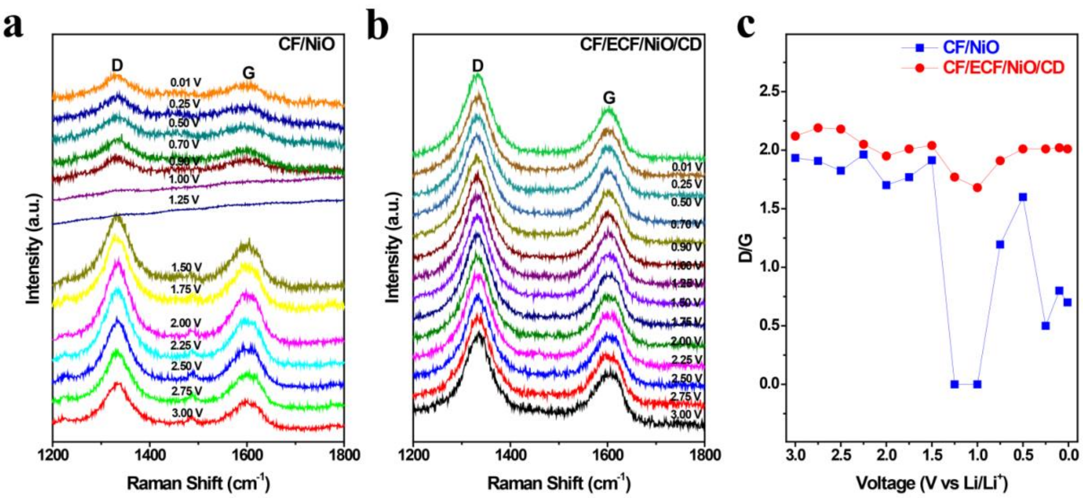

Fig. 4. *In-situ* Raman spectra of a) CF/NiO and b) CF/ECF/NiO/CD at different intercalated voltages. c) Plot of the ID/IG vs. intercalated voltages of CF/NiO and CF/ECF/NiO/CD cells.

The inferior performance of CF/NiO can be attributed to the little or no capacity from the CF current collector electrode. Raman analysis is one of the most vital parameter to study the variation in the D and G bands of carbon materials [22]. Hence, we utilized Raman spectra analysis to study the variation of D and G bands during Li-ion reaction with the both CF/NiO and CF/ECF/NiO/CD. Figure 4a and 4b display the Raman spectra of CF/NiO and CF/ECF/NiO/CD at different Li-ion insertion voltages ranging from 3.0 V to 0.01 V, respectively. The D:G value collected at each voltage were plotted against the corresponding voltages. Figure 4c shows that upon Li-ion intercalation into both CF/NiO and CF/ECF/NiO/CD between 3.0 and 1.5 V, the voltage-D:G plots almost remain the same for both cells (approximately 2.0). Between 1.5 V and 1.0 V, the D:G values are zero for CF/NiO cell due to Li-ion intercalation into the NiO structure. This indicates that the CF displays little or less contribution to the Li-storage process of CF/NiO. However, the D:G values at these voltages for CF/ECF/NiO/CD slightly reduces (1.77 and 1.68) indicating that CF/ECF greatly contributed to the Li-storage process of

CF/ECF/NiO/CD anode and also suggesting the interaction between CF/ECF and NiO. Our previous work shows that the D:G value during Li-ion intercalation at 1.0 V is also zero [22] and we could relate such phenomenon to the slight loss in the cell capacity due to the poor conductivity and stability of such TMO. However, we address such phenomenon in this present work by coating CDs on the nanostructure interface to relief the poor conductivity and stability of NiO, which could reduce capacity loss, improve electrochemical reactivity and enhance CE towards achieving highly stable and highly conductive monolithic electrode [44]. As the discharge process proceeds to 0.5 V and below, the D:G values of CF/ECF/NiO/CD increases and maintains the same values with those of high voltage region indicating capacity contribution from CF/ECF substrate. However, reverse is the case for CF/NiO because the D:G value reduces to 0.4 upon complete discharging process, which can be observed from the weak D and G peaks according Figure 4a compared to that of CF/ECF/NiO/CD. Low D:G value at low discharge voltage in CF/NiO cell indicates that intercalation of Li-ion into the CF cavity shows less capacity contribution to the entire electrode. Hence, the *in situ* Raman spectra results confirmed CF/ECF contributed to the high areal capacity of CF/ECF/NiO/CD electrode.

3.4. Electronic Interaction Study

The synergistic effect between CF/ECF and NiO coupled with coating of CDs plays a crucial part on the excellent Li storage performance of CF/ECF/NiO/CD. Such synergistic effects have been proven to originate from the change in the electronic structure within the hybrids during the electrode design [11, 22]. To confirm this, XPS spectra analyses were employed for further verification. According to C 1s XPS spectra, the C-C bond of both CF/ECF/NiO and CF/ECF/NiO/CD exhibited a positive binding energy shift (Figure 5a), while the entire Ni 2p XPS spectra exhibited a negative binding energy shift (Figure 5b) and CF/ECF/NiO/CD is characterized with the most positive and negative shifts.

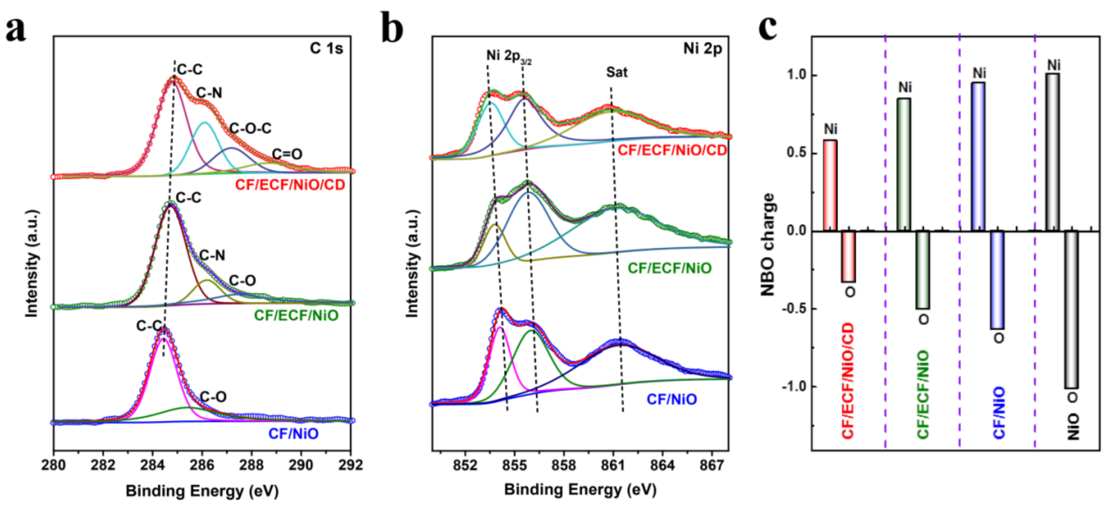

Fig. 5. Electronic interaction characterization. a) C 1s and b) Ni 2p XPS spectra of CF/NiO, CF/ECF/NiO and CF/ECF/NiO/CD. c) NBO Charge density redistributions on CF/NiO, CF/ECF/NiO and CF/ECF/NiO/CD obtained from the theoretical calculations.

Such shifts in the XPS spectra of C and Ni imply a change in the electronic configuration of the samples upon continuous hybridization and created strongest electronic interaction in CF/ECF/NiO/CD when compared with CF/NiO and CF/ECF/NiO. Moreover, it was noted that the characteristic Raman peak around 534 cm^{-1}, which is assigned to the Raman band of NiO [17], as well as those of D and G bands show red-shifts (Figure S8) indicating that the state of bonding in the double-hybrid samples changes due to electronic interactions between CF/ECF, NiO and CD [45].

3.5. Natural Bonding Orbital (NBO) Charge Distribution

The change in the electronic structure and interaction among the samples can further be verified by the variation in the charge distribution of the samples, which can be determined by Density functional theory (DFT) calculations. NiO was also introduced for basic comparisons. The structure model for the DFT calculations of CF, ECF, NiO, CF/NiO, CF/ECF/NiO and CF/ECF/NiO/CD can be found in Figure S15a-f, respectively. The natural bonding orbital (NBO) distribution of the samples is displayed in Figure 5c and the covalent bonding between the C and O functional groups of CF/ECF and NiO is clearly identified in Figure S16. In the electronic structure of CF/ECF/NiO/CD, the charges on both Ni and O becomes less electropositive and less electronegative, respectively (Figure 5c), while the charge on C becomes more electropositive (Figure S17), and reverse is the case for other samples, meaning that the electropositivity and electronegativity in Ni and O increases in the order of CF/ECF/NiO/CD < CF/ECF/NiO < CF/NiO < NiO and the electropositivity in C decreases in the order of CF/ECF/NiO/CD > CF/ECF/NiO > CF/NiO. These results is in accordance with our XPS results further affirming that there exists stronger electronic interaction between each materials in CF/ECF/NiO/CD and the strongest electronic interaction is in the order of CF/ECF/NiO/CD > CF/ECF/NiO > CF/NiO > NiO. Hence, such interaction is responsible for the rapid Li-ion transportation pathway and favorable kinetics in CF/ECF/NiO/CD electrode system.

4. Discussion

4.1. Electron Charge Density and Adsorption Capability

In order to study the adsorption behavior of Li on CF/NiO, CF/ECF/NiO and CF/ECF/NiO/CD hybrids, the difference in the electron density for Li-ion on these hybrids were studied using DFT calculations. Different from CF/NiO hybrid, the slices on oxygen surface in both CF/ECF/NiO and CF/ECF/NiO/CD show accumulation of electrons around the ECF, indicating stronger charge transfer than those of CF/NiO (Figure 6a-c).

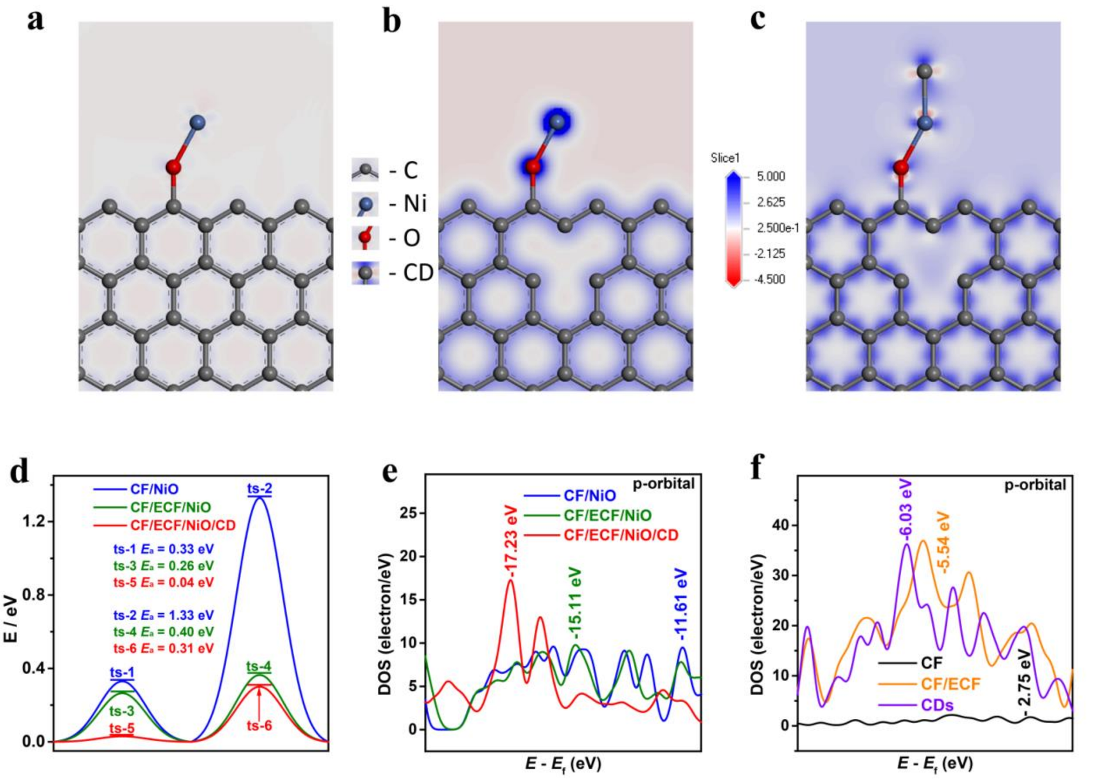

Fig. 6. Mechanism and Theoretical Characterization. Differences of electron charge density for Li on a) CF/NiO, b) CF/ECF/NiO and c) CF/ECF/NiO/CD electrodes. d) Gibb's free adsorption energy (△G) profile of Li-ion intercalation via CF/NiO, CF/ECF/NiO and CF/ECF/NiO/CD. e) DOS plots of CF/NiO, CF/ECF/NiO and CF/ECF/NiO/CD and their corresponding p-bands. f) DOS plots of CF, CF/ECF and CD and their corresponding p-bands.

After CD introduction, the slice on CD surface in the CF/ECF/NiO/CD shows more charge accumulation around the Ni (Figure 6c), implying an enhanced binding energy between the adsorbates and the hybrid surface allowing CF/ECF/NiO/CD to exhibit the strongest charge transfer and adsorption of Li-ion [46]. During Li-ion transportation within the hybrids, the optimal Gibbs free energy change (ΔG_{Li*}) requires for the Li-ion discharge process were determined. The closer the ΔG_{Li*} (E_a, eV) value to zero (0 eV), the faster the transportation of Li-ion and kinetics [47, 48].

The simulations for Li-ion intercalation in CF/NiO, CF/ECF/NiO and CF/ECF/NiO/CD are depicted in Figure S18a-c, respectively. According to Figure 6d, there are two peak regions representing the ΔG_{Li*} for both NiO and C. The ΔG_{Li*} for Li-ion intercalation into NiO-region (denoted as ts-1/3/5 for the 3 electrodes, respectively) reduces in the order of CF/ECF/NiO/CD (0.04 eV) < CF/ECF/NiO (0.26 eV) < CF/NiO (0.33 eV) (Figure 6d). This result implies that the coating of CDs on NiO allows CF/ECF/NiO/CD to attract less adsorption energy leading to enhance rapid transportation of Li-ion and high capacity. Additionally, the ΔG_{Li*} for Li-ion intercalation into C-region (denoted as ts-2/4/6 for the 3 electrodes, respectively) also reduces in the order of CF/ECF/NiO/CD (0.31 eV) < CF/ECF/NiO (0.40 eV) < CF/NiO (1.33 eV) (Figure 6d). It can be observed that the ΔG_{Li*} values of Li-ion intercalation into C are higher than that of NiO, suggesting the lower capacity contribution from C-region compared to that of NiO-region. Moreover, both CF/ECF/NiO/CD and CF/ECF/NiO requires much lesser free energy due to the excellent properties of CF/ECF compared to bare CF and its derivative (CF/NiO).

4.2. Density of States (DOS)

The density of states (DOS) of Li-ion transportation near the Fermi level (E_f) that majorly originates from the p-band adsorption energy state [49], were further analyzed to solidify the electronic interaction between the CF/ECF and the active material NiO (Figure S19). According to Figure S20, the d-orbital center relative to E_f are calculated to be in the order of CF/NiO (-8.77 eV) > CF/ECF/NiO (-7.43 eV) > CF/ECF/NiO/CD (-5.13 eV). However, the p-orbital center relative E_f are determined to be in the order of CF/ECF/NiO/CD (-17.23 eV) > CF/ECF/NiO (-15.11 eV) > CF/NiO (-11.61 eV) (Figure 6e). From these results, we deduced that the introduction of CDs allows the p-band center of CF/ECF/NiO/CD to be far away from E_f, suggesting strong adhesiveness of bonding states and strengthening of the electronic interaction within the CF/ECF/NiO/CD matrix [49]. Impressively, as the relationship between the d-orbital center and E_f of CF, CF/ECF and CDs are zero (Figure S21) the p-orbital center of CF, CF/ECF and CDs relative to E_f are derived to be -2.75 eV, -5.54 eV and -6.03 eV, respectively (Figure 6f), showing that CF/ECF and CD are farther from the E_f than CF. Such phenomenon further explains the reason why CF/ECF/NiO/CD, designed with both CF/ECF and CD, could exhibit the farthest p-orbital center relative to E_f. Hence, the excellent Li storage performance of CF/ECF/NiO/CD emanates from the p-orbital shift, which grants the modulation of the electrochemical behaviour of NiO to be high areal capacity anode for LIBs.

4.3. Mechanism

The schematic representation of the Li-ion transfer depicted in Scheme 1 explained the proposed mechanism for lithium storage capacity enhancement.

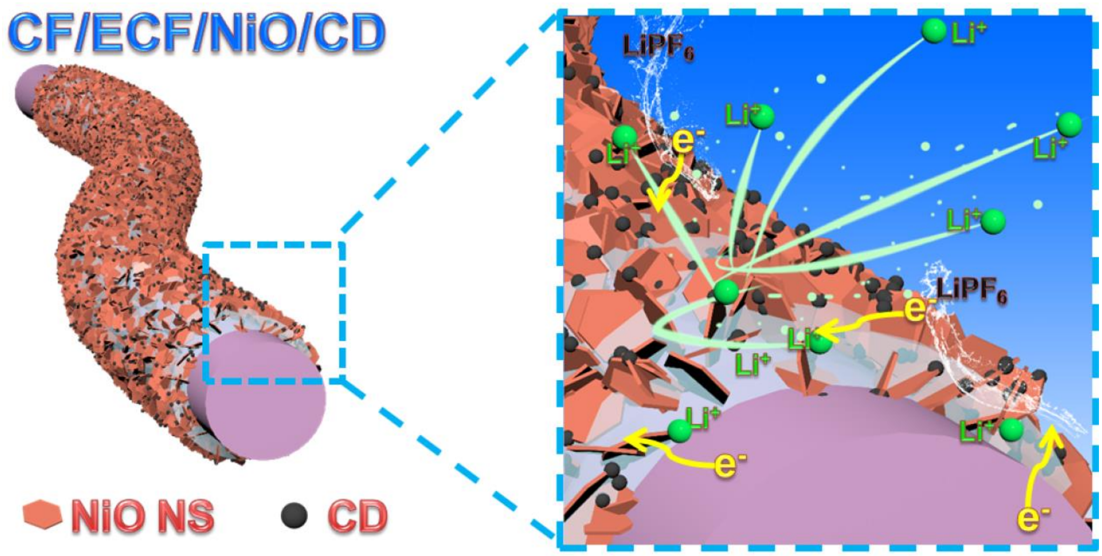

Scheme 1. Simplified interpretation of CF/ECF/NiO/CD anode with bicontinuous Li ion and electron transfer routes.

The CF/ECF/NiO/CD core-multishell battery electrode is designed to allow continuous transfer of electron through CF/ECF, NiO and CD. (a) The porosity of the

3D CF/ECF attracts higher surface area which is beneficial for the introduction of more active sites as well as the interface of electrode/electrolyte towards easy and rapid absorption of Li-ion and electron transfer. The CF/ECF plays the role of current collector/substrate, capacity contributor and excellent lighter free-standing and flexible scaffold. (b) The good adhesion of the porous NiO nanosheets to the porous exfoliated surface of CF/ECF allows strong electronic interaction between the CF/ECF and NiO nanosheets, which could enhances the diffusion of ion and kinetics of charge transportation towards high-rate performance and applications. (c) The coating of CDs that serves the following functions; (i) Because most TMOs are well known to exhibits poor conductivity and stability [6, 41], CDs enhances the conductivity of NiO nanosheets, which is very essential for further improving the kinetics of the entire electrode architecture leading to excellent cyclic and rate capability. (ii) as a protector for both the NiO nanosheets and entire multihybrid system i.e. protecting the NiO nanosheets from easy agglomeration leading to the minimization of active materials dissolution during cyclic stability performance and (iii) improves the coulombic efficiency (CE) and capacity of CF/ECF/NiO/CD. Hence, such architecture is monolithic in nature allowing easy entrance of electrolyte to both sides of the nanosheets during Li-ion intercalation process, which create more opportunity for Li-ion and electrons to directly react with NiO.

5. Full-cell Lithium Ion Batteries

Based on the fact that CF/ECF/NiO/CD exhibits the excellent areal capacity as anode material for LIBs, we utilized CF/ECF/NiO/CD anode in the fabrication of full coin-cell LIBs and compare their performance with that of CF/NiO anode. Commercial LNCMO casted on CF/ECF (denoted CF/ECF/LNCMO) was employed as cathode for reasonable comparison. Our previous work has shown that LNCMO casted on CF/ECF displayed better Li-storage performance than that casted on CF as cathode material for LIBs [22]. CF/ECF/NiO/CD//CF/ECF/LNCMO battery was then scaled-up to 45.0 cm^2 soft-pack flexible battery design. The electrolyte/electrode ratio is 2.3 g Ah^{-1} indicating that 2.3 g of 1 M $LiPF_6$ (containing 1:1 by volume of EC/DMC) is required to achieve 1 Ah specific capacity. The digital image of the scale-up soft-pack flexible battery shows that the thickness of the battery is 0.10 cm as shown in Figure S22. According to the charge-discharge curves (Figure 7a) and CV curves (Figure S23) of devices, the working voltages of both CF/NiO-based and CF/ECF/NiO/CD-based batteries are 3.50 V. The CF/ECF/NiO/CD//CF/ECF/LNCMO LIB could achieve an areal capacity of 41.33 mAh cm^{-2} at current density of 5 mA, which is significantly higher than the CF/NiO-based LIB (30.68 mAh cm^{-2}). The energy efficiency of the two batteries, which depends on the overpotentials of galvanostatic curves in Figure 7a (i.e. the area beneath the galvanostatic curves) and were calculated based on the formula below[50-52];

$$\text{Energy efficiency} = \frac{\text{Energy density}_{(discharge)}}{\text{Energy density}_{(charge)}} \text{ x } 100\% \quad (3)$$

Thus, the energy efficiency of the CF/ECF/NiO/CD-based LIB is 93%, which is also higher than the CF/NiO-based LIB. At current value of 5 mA, the CF/ECF/NiO/CD-based LIB exhibit excellent stability capacity of 40.89 mAh cm^{-2} (i.e. retaining 98% of its initial capacity at 41.62 mAh cm^{-2}) after 300 electrochemical cycles, unlike that of CF/NiO//CF/ECF/LNCMO, which could only deliver a capacity of 19.56 mAh cm^{-2} (i.e. 63% of its initial capacity at 30.68 mAh cm^{-2} (Figure 7b). Thus, the superior stability of CF/ECF/NiO/CD over CF/NiO can both be confirmed in the half and full cell LIBs.

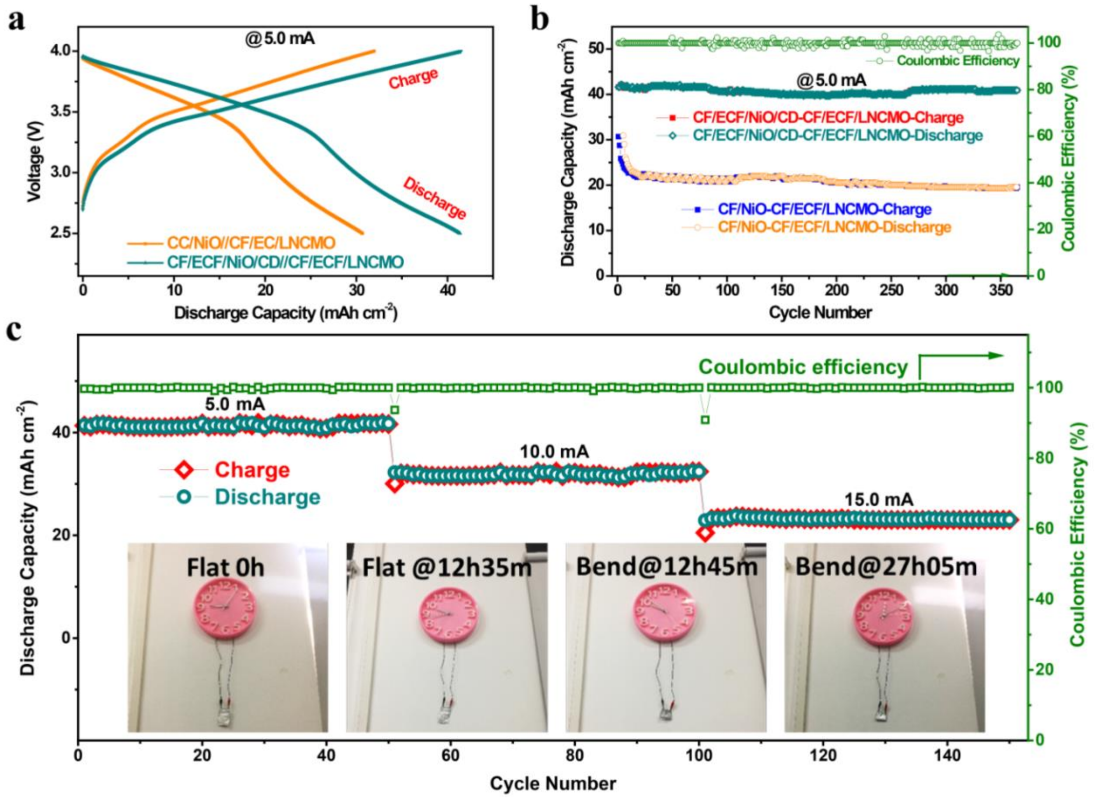

Fig. 7. Flexible full cell properties of the soft-pack flexible LIB soft-pack flexible LIB. a) Charge-discharge profiles and b) cyclic stability of CF/NiO//CF/ECF/LNCMO and CF/ECF/NiO/CD//CF/ECF/LNCMO full coin-cell batteries. c) Cycling rate capability of CF/ECF/NiO/CD//CF/ECF/LNCMO soft-pack flexible LIB at the applied currents of 5.0, 10.0 and 15.0 mA. Inset in “c” is the potential application of the soft-pack flexible LIB powering a wall-clock for 27 h at both flat and bending states.

Finally, the CF/ECF/NiO/CD//CF/ECF/LNCMO FLIB was subjected to different current values of 5.0, 10.0 and 15.0 mA for 50 cycles each at after 50 folding and at 180^o bending angle. The flexible battery still retain its capacity delivering a high areal capacity of 41.33 mAh cm^{-2} when current of 5.0 mA was applied, which are equivalent to 413.3 mAh cm^{-3} (based on the thickness of the soft-pack battery, 0.1 cm) and 134.5 mAh g^{-1} (based on the entire weight of the battery, 308 mg) Figure S24, S25 and Table S1]. The battery could also operate successfully at increasing current value up to 15 mA retaining an areal capacity of 12.59 mAh cm^{-2} (125.9 mAh cm^{-3} and 115.8 mAh g^{-1}). The flexible battery also maintained outstanding flexible stability up to 150 cycle (Figure 7c) and could also achieve a 201.7 Wh kg^{-1} (619.9 Wh L^{-1}) based on the entire weight of the battery. The CF/ECF/NiO/CD//CF/ECF/LNCMO LIB could power a wall-clock at the flat and bending states for more than 27 h after stability test owing to the flexibility of both the anode and cathode materials (Figure 7c inset). This suggests great potential application for flexible energy storage devices. Video demonstration of the device driving a wall clock at the flat and bending conditions before and after 27 h can be found in Figure SV1 and Figure SV2, respectively.

6. Conclusions

In conclusion, we have successfully established that constructing 3D self-standing and *monolithic* electrode could enhance the areal capacity of LIB not only due to the capacity contribution from the surface functionalized flexible carbon fiber but also by tailoring the p-orbital center. The 3D monolithic flexible anode that consists of carbon fiber coated with N-doped porous exfoliated carbon fiber, NiO and CDs (denoted CF/ECF/NiO/CD) exhibits a high reversible areal capacity of 3.97 mAh cm^{-2} at 0.25 mA cm^{-2}, excellent rate performance capacity of 2.61 mAh cm^{-2} at 6.0 mA cm^{-2} and impressive stability retention capacity of 2.90 mAh cm^{-2} after 250 electrochemical cycles. *In-situ* Raman, XPS and DFT studies persistently confirm that the improved Li-storage performance can be related to the capacity contribution from the flexible carbon-based current collector, coating of the CDs and shift in the p-orbital leading to strong electronic interaction within the CF/ECF/NiO/CD systems. Moreover, CF/ECF/NiO/CD was easily scaled-up as anode material to design a

45.0 cm^2 soft-pack full LIB battery using commercial LNCMO as cathode. The soft-pack CF/ECF/NiO/CD-based LIBs delivers a high areal capacity, volumetric capacity and mass capacity of 41.33 mAh cm^{-2}, 413.3 mAh cm^{-3} and 134.5 mAh g^{-1}, respectively (equivalent to high energy density at 619.9 Wh L^{-1} or 201.7 Wh kg^{-1}) at high current density of 5 mA, showing a great potential application in developing high areal capacity flexible energy storage devices.

Acknowledgements

This work was supported by the Natural Science Foundation of China (21875292 and 21773315), Science Starting Foundation of Hunan University (531118010182) and China Postdoctoral Science Foundation (2018M640847 and 2019T120764).

Conflict of interest

The authors declare no competing financial interest.

References

[1] J. Ma, J. Sung, J. Hong, S. Chae, N. Kim, S.-H. Choi, G. Nam, Y. Son, S.Y. Kim, M. Ko, J. Cho, Towards maximized volumetric capacity via pore-coordinated design for large-volume-change lithium-ion battery anodes, Nat. Commun. 10 (2019) 475.

[2] J. Zheng, Q. Zhao, X. Liu, T. Tang, D.C. Bock, A.M. Bruck, K.R. Tallman, L.M. Housel, A.M. Kiss, A.C. Marschilok, E.S. Takeuchi, K.J. Takeuchi, L.A. Archer, Nonplanar Electrode Architectures for Ultrahigh Areal Capacity Batteries, ACS Energy Lett. 4 (2019) 271-275.

[3] L. Sheng, S. Liang, T. Wei, J. Chang, Z. Jiang, L. Zhang, Q. Zhou, J. Zhou, L. Jiang, Z. Fan, Space-confinement of MnO nanosheets in densely stacked graphene:

Ultra-high volumetric capacity and rate performance for lithium-ion batteries, Energy Stor. Mater. 12 (2018) 94-102.

[4] B. Wang, J. Ryu, S. Choi, G. Song, D. Hong, C. Hwang, X. Chen, B. Wang, W. Li, H.-K. Song, S. Park, R.S. Ruoff, Folding Graphene Film Yields High Areal Energy Storage in Lithium-Ion Batteries, ACS Nano 12 (2018) 1739-1746.

[5] Y. Lu, L. Yu, X.W. Lou, Nanostructured Conversion-type Anode Materials for Advanced Lithium-Ion Batteries, Chem 4 (2018) 972-996.

[6] M. Zheng, H. Tang, L. Li, Q. Hu, L. Zhang, H. Xue, H. Pang, Hierarchically Nanostructured Transition Metal Oxides for Lithium-Ion Batteries, Adv. Sci. 5 (2018) 1700592.

[7] X. Tang, G. Chen, Z. Mo, D. Ma, S. Wang, J. Wen, L. Gong, L. Zhao, J. Huang, T. Huang, J. Luo, Controllable two-dimensional movement and redistribution of lithium ions in metal oxides, Nat. Commun. 10 (2019) 2888.

[8] N. Nitta, F. Wu, J.T. Lee, G. Yushin, Li-ion battery materials: present and future, Materials Today 18 (2015) 252-264.

[9] M. Li, J. Lu, Z. Chen, K. Amine, 30 Years of Lithium-Ion Batteries, Adv. Mater. 30 (2018) 1800561.

[10] M.-S. Balogun, W. Qiu, Y. Luo, H. Meng, W. Mai, A. Onasanya, T.K. Olaniyi, Y. Tong, A review of the development of full cell lithium-ion batteries: The impact of nanostructured anode materials, Nano Res. 9 (2016) 2823-2851.

[11] Y.-F. Li, Y.-H. Shi, S.-G. Wang, J.-H. Liu, J. Lin, Y. Xia, X.-L. Wu, C.-Y. Fan, J.-P. Zhang, H.-M. Xie, H.-Z. Sun, Z.-M. Su, Carbon/Binder-Free NiO@NiO/NF with In Situ Formed Interlayer for High-Areal-Capacity Lithium Storage, Adv. Energy Mater. 9 (2019) 1803690.

[12] F. Zhang, C. Yang, H. Guan, Y. Hu, C. Jin, H. Zhou, L. Qi, 3D Copper Foam@FeO_x Nanoarrays as a High Areal Capacity and Stable Electrode for Lithium-Ion Batteries, ACS Applied Energy Materials 1 (2018) 5417-5427.

[13] L. Li, H.B. Wu, L. Yu, S. Madhavi, X.W. Lou, A General Method to Grow Porous α-Fe_2O_3 Nanosheets on Substrates as Integrated Electrodes for Lithium-Ion Batteries, Adv. Mater. Interfaces 1 (2014) 1400050.

[14] R. Elango, A. Demortière, V. De Andrade, M. Morcrette, V. Seznec, Thick Binder-Free Electrodes for Li–Ion Battery Fabricated Using Templating Approach and Spark Plasma Sintering Reveals High Areal Capacity, Adv. Energy Mater. 8 (2018) 1703031.

[15] X. Han, Z. Zhang, G. Zheng, R. You, J. Wang, C. Li, S. Chen, Y. Yang, Scalable Engineering of Bulk Porous Si Anodes for High Initial Efficiency and High-Areal-Capacity Lithium-Ion Batteries, ACS Appl. Mater. Interfaces 11 (2019) 714-721.

[16] Y. Yue, H. Liang, 3D Current Collectors for Lithium-Ion Batteries: A Topical Review, Small Methods 2 (2018) 1800056.

[17] M.-S. Balogun, W. Qiu, Y. Luo, Y. Huang, H. Yang, M. Li, M. Yu, C. Liang, P. Fang, P. Liu, Y. Tong, Improving the Lithium-Storage Properties of Self-Grown Nickel Oxide: A Back-Up from TiO_2 Nanoparticles, ChemElectroChem 2 (2015) 1243-1248.

[18] J. Zhu, Q. Wu, J. Key, M. Wu, P.K. Shen, Self-assembled superstructure of carbon-wrapped, single-crystalline Cu_3P porous nanosheets: One-step synthesis and enhanced Li-ion battery anode performance, Energy Stor. Mater. 15 (2018) 75-81.

[19] J. Zhan, S. Deng, Y. Zhong, Y. Wang, X. Wang, Y. Yu, X. Xia, J. Tu, Exploring hydrogen molybdenum bronze for sodium ion storage: Performance enhancement by vertical graphene core and conductive polymer shell, Nano Energy 44 (2018) 265-271.

[20] Z. Deng, H. Jiang, Y. Hu, Y. Liu, L. Zhang, H. Liu, C. Li, 3D Ordered Macroporous MoS_2@C Nanostructure for Flexible Li-Ion Batteries, Adv. Mater. 29 (2017) 1603020-1603026.

[21] X. Min, B. Sun, S. Chen, M. Fang, X. Wu, Y.g. Liu, A. Abdelkader, Z. Huang, T. Liu, K. Xi, R. Vasant Kumar, A textile-based SnO_2 ultra-flexible electrode for lithium-ion batteries, Energy Stor. Mater. 16 (2019) 597-606.

[22] M.-S. Balogun, H. Yang, Y. Luo, W. Qiu, Y. Huang, Z.-Q. Liu, Y. Tong, Achieving high gravimetric energy density for flexible lithium-ion batteries facilitated by core–double-shell electrodes, Energy Environ. Sci. 11 (2018) 1859-1869.

[23] M.-S. Balogun, Y. Luo, F. Lyu, F. Wang, H. Yang, H. Li, C. Liang, M. Huang, Y. Huang, Y. Tong, Carbon Quantum Dot Surface-Engineered VO_2 Interwoven Nanowires: A Flexible Cathode Material for Lithium and Sodium Ion Batteries, ACS Appl. Mater. Interfaces 8 (2016) 9733-9744.

[24] G. Kresse, J. Furthmüller, Efficient iterative schemes for ab initio total-energy calculations using a plane-wave basis set, Phys. Rev. B 54 (1996) 11169-11186.

[25] J.P. Perdew, K. Burke, M. Ernzerhof, Generalized Gradient Approximation Made Simple, Phys. Rev. Lett. 77 (1996) 3865-3868.

[26] S. Grimme, Semiempirical GGA-type density functional constructed with a long-range dispersion correction, J. Comput. Chem. 27 (2006) 1787-1799.

[27] E. Sanville, S.D. Kenny, R. Smith, G. Henkelman, Improved grid-based algorithm for Bader charge allocation, J. Comput. Chem. 28 (2007) 899-908.

[28] M.-S. Balogun, W. Qiu, F. Lyu, Y. Luo, H. Meng, J. Li, W. Mai, L. Mai, Y. Tong, All-flexible lithium ion battery based on thermally-etched porous carbon cloth anode and cathode, Nano Energy 26 (2016) 446-455.

[29] S. Xie, H. Su, W. Wei, M. Li, Y. Tong, Z. Mao, Remarkable photoelectrochemical performance of carbon dots sensitized TiO_2 under visible light irradiation, J. Mater. Chem. A 2 (2014) 16365-16368.

[30] W. Li, Y. Liu, M. Wu, X. Feng, S.A.T. Redfern, Y. Shang, X. Yong, T. Feng, K. Wu, Z. Liu, B. Li, Z. Chen, J.S. Tse, S. Lu, B. Yang, Carbon-Quantum-Dots-Loaded Ruthenium Nanoparticles as an Efficient Electrocatalyst for Hydrogen Production in Alkaline Media, Adv. Mater. 30 (2018) 1800676.

[31] J. Briscoe, A. Marinovic, M. Sevilla, S. Dunn, M. Titirici, Biomass-Derived Carbon Quantum Dot Sensitizers for Solid-State Nanostructured Solar Cells, Angew. Chem. Int. Ed. 54 (2015) 4463-4468.

[32] D. Su, H.-S. Kim, W.-S. Kim, G. Wang, Mesoporous Nickel Oxide Nanowires: Hydrothermal Synthesis, Characterisation and Applications for Lithium-Ion Batteries and Supercapacitors with Superior Performance, Chem. Eur. J. 18 (2012) 8224-8229.

[33] H. Song, J. Su, C. Wang, In Situ Subangstrom-Thick Organic Engineering Enables Mono-scale, Ultrasmall ZnO Nanocrystals for a High Initial Coulombic Efficiency, Fully Reversible Conversion, and Cycle-Stable Li-Ion Storage, Adv. Energy Mater. 0 1900426.

[34] R. Hu, Y. Ouyang, T. Liang, X. Tang, B. Yuan, J. Liu, L. Zhang, L. Yang, M. Zhu, Inhibiting grain coarsening and inducing oxygen vacancies: the roles of Mn in achieving a highly reversible conversion reaction and a long life SnO_2–Mn–graphite ternary anode, Energy Environ. Sci. 10 (2017) 2017-2029.

[35] J. Li, S. Hwang, F. Guo, S. Li, Z. Chen, R. Kou, K. Sun, C.-J. Sun, H. Gan, A. Yu, E.A. Stach, H. Zhou, D. Su, Phase evolution of conversion-type electrode for lithium ion batteries, Nat. Commun. 10 (2019) 2224.

[36] C. Guan, X. Wang, Q. Zhang, Z. Fan, H. Zhang, H.J. Fan, Highly stable and reversible lithium storage in SnO_2 nanowires surface coated with a uniform hollow shell by atomic layer deposition, Nano Lett. 14 (2014) 4852-4858.

[37] Y. Luo, M.-S. Balogun, W. Qiu, R. Zhao, P. Liu, Y. Tong, Sulfurization of FeOOH nanorods on a carbon cloth and their conversion into Fe_2O_3/Fe_3O_4-S core-shell nanorods for lithium storage, Chem. Commun. 51 (2015) 13016-13019.

[38] M.-S. Balogun, W. Qiu, J. Jian, Y. Huang, Y. Luo, H. Yang, C. Liang, X. Lu, Y. Tong, Vanadium Nitride Nanowire Supported SnS_2 Nanosheets with High Reversible Capacity as Anode Material for Lithium Ion Batteries, ACS Appl. Mater. Interfaces 7 (2015) 23205-23215.

[39] W. Qiu, M.-S. Balogun, Y. Luo, K. Chen, Y. Zhu, X. Xiao, X. Lu, P. Liu, Y. Tong, Three-dimensional Fe_3O_4 Nanotube Array on Carbon Cloth Prepared from A Facile Route for Lithium ion Batteries, Electrochim. Acta 193 (2016) 32-38.

[40] X. Huang, G. Diao, S. Li, M.-S. Balogun, N. Li, Y. Huang, Z.-Q. Liu, Y. Tong, Enhanced lithium storage performance of porous exfoliated carbon fibers via anchored nickel nanoparticles, RSC Adv. 8 (2018) 17056-17059.

[41] Y. Zhao, X. Li, B. Yan, D. Xiong, D. Li, S. Lawes, X. Sun, Recent Developments and Understanding of Novel Mixed Transition-Metal Oxides as Anodes in Lithium Ion Batteries, Adv. Energy Mater. 6 (2016) 1502175.

[42] D. Chao, C. Zhu, X. Xia, J. Liu, X. Zhang, J. Wang, P. Liang, J. Lin, H. Zhang, Z.X. Shen, Graphene Quantum Dots Coated VO_2 Arrays for Highly Durable Electrodes for Li and Na Ion Batteries, Nano Lett. 15 (2014) 565-573.

[43] X. Wang, L. Lv, Z. Cheng, J. Gao, L. Dong, C. Hu, L. Qu, High-Density Monolith of N-Doped Holey Graphene for Ultrahigh Volumetric Capacity of Li-Ion Batteries, Adv. Energy Mater. 6 (2016) 1502100.

[44] M. Jing, J. Wang, H. Hou, Y. Yang, Y. Zhang, C. Pan, J. Chen, Y. Zhu, X. Ji, Carbon quantum dot coated Mn_3O_4 with enhanced performances for lithium-ion batteries, J. Mater. Chem. A 3 (2015) 16824-16830.

[45] J.-X. Feng, J.-Q. Wu, Y.-X. Tong, G.-R. Li, Efficient Hydrogen Evolution on Cu Nanodots-Decorated Ni_3S_2 Nanotubes by Optimizing Atomic Hydrogen Adsorption and Desorption, J. Am. Chem. Soc. 140 (2018) 610-617.

[46] C. Chen, X. Xie, B. Anasori, A. Sarycheva, T. Makaryan, M. Zhao, P. Urbankowski, L. Miao, J. Jiang, Y. Gogotsi, MoS_2-on-MXene Heterostructures as Highly Reversible Anode Materials for Lithium-Ion Batteries, Angew. Chem. Int. Ed. 57 (2018) 1846-1850.

[47] Y. Chu, L. Guo, B. Xi, Z. Feng, F. Wu, Y. Lin, J. Liu, D. Sun, J. Feng, Y. Qian, S. Xiong, Embedding MnO@Mn_3O_4 Nanoparticles in an N-Doped-Carbon Framework Derived from Mn-Organic Clusters for Efficient Lithium Storage, Adv. Mater. 30 (2018) 1704244.

[48] K. Xu, X. Liu, J. Liang, J. Cai, K. Zhang, Y. Lu, X. Wu, M. Zhu, Y. Liu, Y. Zhu, G. Wang, Y. Qian, Manipulating the Redox Kinetics of Li–S Chemistry by Tellurium Doping for Improved Li–S Batteries, ACS Energy Lett. 3 (2018) 420-427.

[49] J. Zhou, X. Liu, L. Zhu, J. Zhou, Y. Guan, L. Chen, S. Niu, J. Cai, D. Sun, Y. Zhu, J. Du, G. Wang, Y. Qian, Deciphering the Modulation Essence of p Bands in Co-Based Compounds on Li-S Chemistry, Joule 2 (2018) 2681-2693.

[50] Y. Cao, M. Li, J. Lu, J. Liu, K. Amine, Bridging the academic and industrial metrics for next-generation practical batteries, Nat. Nanotechnol. 14 (2019) 200-207.

[51] A. Eftekhari, Energy efficiency: a critically important but neglected factor in battery research, Sustainable Energy & Fuels 1 (2017) 2053-2060.

[52] L. Hu, Y. Gao, T. Xiong, D. Adekoya, W. Qiu, H. Yang, M.S. Balogun, S. Zhang, A. Pan, Y. Li, Y. Tong, Surface functionalized 3D carbon fibers boosts the lithium storage behaviour of transition metal oxide nanowires via strong electronic interaction and tunable adsorption energy, Nanoscale Horiz. 4 (2019) 1402-1410.